Ca^{2+}-dependent nanodomain enrichment is crucial for the perception of bacterial outer membrane vesicles in plants

Ishani Mondal[1], Hrimeeka Das[1,2], Smrutisanjita Behera*[1,2].

[1] Infectious Diseases and Immunology Division, CSIR-Indian Institute of Chemical Biology, 4, Raja S. C. Mullick Road, Kolkata-700032, India.

[2] Academy of Scientific and Innovative Research (AcSIR), Ghaziabad, India

*For correspondence (email: smrutisanjita@gmail.com, sbehera.iicb@csir.res.in)

Summary:

Outer membrane vesicles (OMVs) of Gram-negative bacteria play a crucial role in virulence, communication, and survival. In plants, OMVs induce an immune response. Also, OMVs have been utilised to prime plants against the pathogen. However, a thorough understanding of plant-bacterial interaction via OMVs is still less explored. Our research aims to comprehend the underlying events during the perception of *Xanthomonas oryzae pv. oryzae* (*Xoo*)-OMVs by the host plant, rice (*Oryza sativa subsp. indica*). We have identified that *Xoo*-OMVs contain virulence-associated proteins, MAMPs, cell wall-degrading enzymes, nutrient-acquisition proteins, and proteins to defend the bacteria against the host immune response. We establish that *Xoo*-OMVs can elevate cellular calcium (Ca^{2+}) concentration in rice. We report that this early Ca^{2+} signal is essential for nanodomain enrichment in the rice plasma membrane after exposure to *Xoo*-OMVs. We have observed that *Xoo*-OMVs get incorporated into the plasma membrane of rice. Our results assert that the insertion of *Xoo*-OMVs into the plasma membrane of rice is also a Ca^{2+}-dependent process. Moreover, we establish that with the chelation of Ca^{2+}, the resistant rice seedlings exhibit a weakened immune response against *Xoo*-OMVs. Taken together, our study reveals the early events of *Xoo*-OMV perception by rice via the Ca^{2+} signal.

Significance Statement:

Our research describes the early events of *Xoo*-OMV perception by rice. It establishes that *Xoo*-OMVs induce a Ca^{2+} signal in rice. This OMV–induced Ca^{2+} signal initiates a relay of events, including nanodomain enrichment, followed by the insertion of *Xoo*-OMVs into the rice plasma membrane. This study contributes to the knowledge that can be utilized in OMV engineering for plant protection. Importantly, our work conceptualizes Ca^{2+}-dependent nanodomain development, which will aid in interrelating various signalling pathways in the future.

Introduction

Gram-negative bacteria produce vesicles that are released into their surroundings, known as outer membrane vesicles (OMVs) (Beveridge, 1999). OMVs are spherical, nanosized proteo-liposomes produced by blebbing of the outer membrane of the gram-negative bacteria (Jan, 2017; Schwechheimer and Kuehn, 2015). Outer membrane proteins (OMPs), toxins, glycoproteins, enzymes, virulence factors, lipopolysaccharide (LPS), and even nucleic acids

are important constituents of OMVs (Altindis et al., 2014; Buck et al., 2014; Jang et al., 2014; Lee et al., 2008, 2007; Renelli et al., 2004) that help in biofilm formation, quorum sensing, virulence, communication, etc., thereby helping the bacteria to adapt to their surroundings (Kulp and Kuehn, 2010; McBroom and Kuehn, 2007; Sartorio et al., 2021).

OMVs isolated from *E. coli* have been engineered to deliver proteins into the mouse cells (Chen et al., 2010), and OMV-based vaccines have been successfully developed in the case of *N. meningitidis group B (MenB)* (Sartorio et al., 2021). Chalupowicz et al. demonstrated the immune-protective function of *Xcc*-OMVs. Pre-treatment of Arabidopsis plants with *Xcc*-OMV reduces the growth of the pathogen in the host (Chalupowicz et al., 2023). Similarly, it is reported that pre-treatment of OMVs isolated from *Pseudomonas syringae pv. tomato (Pst)* can protect the tomato plant from subsequent infection (McMillan and Kuehn, 2023). This evidence supports the possibility of utilising OMVs to combat the widespread bacterial diseases in plants. However, the role of OMVs in plant-pathogen interaction remains obscure compared to their animal counterpart. OMVs isolated and characterised from phytopathogenic bacteria, including *Xylella fastidiosa and Xanthomonas campestris pv. campestris* (*Xcc*), *Pseudomonas syringae pv. tomato*, *Pectobacterium brasiliense*, and *Candidatus liberibacter* (Chowdhury and Jagannadham, 2013; Huang et al., 2022; Maphosa and Moleleki, 2021; Mendes et al., 2016; Sidhu et al., 2008) carry outer membrane proteins (OMPs), toxins, cell wall-degrading enzymes, porins, lipases, etc. and virulence factors like T3SS secretion proteins (Chowdhury and Jagannadham, 2013; Jang et al., 2014; Sidhu et al., 2008). Moreover, OMVs produced by *Xanthomonas campestris pv. campestris* (*Xcc*-OMVs) carry MAMPs like flg22, EF-Tu, etc. (Bahar et al., 2016; Feitosa-Junior et al., 2019). Importantly, A recent report has shown that *Pst* DC3000 OMVs carry ROS-protecting enzyme KatB to protect the host against host immune responses (Deng et al., 2025). Nevertheless, the mechanism of perception of the pathogenic bacteria by the plants is still unexplored. OMVs have been shown to trigger ROS bursts and elicit a PRR-mediated immune response in host plants (Bahar et al., 2016; Chalupowicz et al., 2023; Tran et al., 2022). Interestingly, RNAseq analysis of *Xcc*-OMV-treated Arabidopsis plants confirms a major transcriptional shift towards immune system activation (Chalupowicz et al., 2023). Notably, the comparison between the transcriptome performed by *Xcc*-OMV treatment and individual elicitor treatment in Arabidopsis induces a common set of gene activation, along with the activation of some unique pathways exclusively in *Xcc*-OMV-treated plants (Chalupowicz et al., 2023). This suggests that plants may perceive bacterial OMV as a specific PAMP. To understand this, a thorough understanding of OMV-induced early signalling events in the plants is required. One of the known early signalling events is the membrane nanodomain enrichment in Arabidopsis after *Xcc*-OMV application. Tran et al. proposed that the *Xcc*-OMVs get inserted into the host plasma membrane through nanodomain enrichment (Tran et al., 2022). Further study will elucidate the nanodomain enrichment process by bacterial OMVs.

Nanodomains are nanoscale proteo-lipid congregations at the plasma membrane that are key players in plants during the perception of various biotic and abiotic stress (Gronnier et al., 2017; Jaillais and Ott, 2020; Nagano et al., 2016). Nanodomain potentiation is a crucial event during plant immune signalling (Ott, 2017). Nanodomains guide the spatiotemporal specificity of the FLS2 and BRI1 pathways in Arabidopsis (Bücherl et al., 2017). During osmotic stress,

the segregation of ROP6 and NADPH oxidases into specialized nanodomains in the Arabidopsis plasma membrane is critical for ROS burst response and subsequent downstream signalling (Smokvarska et al., 2020). *Xcc*-OMVs induce nanodomain enrichment in the Arabidopsis plasma membrane (Tran et al., 2022). However, the underlying mechanism of this nanodomain enrichment is yet to be deciphered.

Ca^{2+} is indispensable for a plant's immune response. Stimulus-specific Ca^{2+} signatures have been observed in plant cells in response to MAMPs like flg22, chitin, elf18, and pep1 (Cao et al., 2017; Keinath et al., 2015; Ranf et al., 2014). A sustained Ca^{2+} increase is observed during the HR response in Arabidopsis challenged by *Pseudomonas syringae* (Grant et al., 2000). Ca^{2+} permeable channels like CNGC2 and CNGC4 are important in shaping PTI-induced Ca^{2+} signals (Ali et al., 2007; Tian et al., 2019). Intriguingly, the Ca^{2+}-dependent protein kinase CPK3 can influence the function of the group 1 REMORIN REM1.3, a PM nanodomain-associated protein, by phosphorylating the intrinsically disordered domain (IDD) of REM1.3 (Perraki et al., 2018). These evidences suggest that both Ca^{2+} and nanodomain congregation are crucial events for immune signalling in plants. It would be interesting to investigate if OMVs released by phytopathogenic bacteria also employ Ca^{2+}-mediated signalling pathways to carry out their function in plants.

In this work, we have explored the early events during Xanthomonas oryzae pv. oryzae (*Xoo*)-rice interaction to apprehend the mode of OMV perception by plants. *Xoo* is a gram-negative bacterium that causes Bacterial Blight of rice, leading to a significant loss of rice yield, an economically important crop (Niño-Liu et al., 2006). We have isolated OMVs from *Xoo* and examined how rice (*Oryza sativa subsp. indica*) responds when exposed to *Xoo*-OMVs. To this end, we have used one susceptible variety of rice, namely, Khitish, and a resistant variety of rice called CR 800. The CR 800 variety expresses three R genes- *xa13, xa5,* and *Xa21,* which render it resistant to *Xoo* infection (Mohapatra et al., 2023). We have studied the early defence responses employed by Khitish and CR 800 against *Xoo*-OMVs. We have found that *Xoo*-OMVs carry abundant MAMPs like EF-Tu, flagellin, Ax21, etc. This prompted us to enquire about the generation of Ca^{2+} signal in plants in response to *Xoo*-OMVs. We have discovered an *Xoo*-OMV-induced Ca^{2+} elevation in both Khitish and CR 800. We have further witnessed that *Xoo*-OMVs can incite a rapid increase in the lipid order of the host plasma membrane and get inserted into the plasma membrane in a Ca^{2+}-dependent manner. Collectively, our results describe the Ca^{2+}-dependent relay of events during the perception of OMVs by the host plant and contribute to the understanding of early host-pathogen interaction.

Results:

1. *Xoo*-OMV*s* carry several MAMPs and virulence-associated proteins

Xanthomonas oryzae pv. oryzae OMVs were isolated for the first time from the PXO99A strain by Bahar et al., in 2016. They had visualized the OMVs through transmission electron microscopy (TEM) (Bahar et al., 2016), however no further study was performed on the OMVs of this rice pathogen. In this study, we isolated OMVs from *Xoo* strain BXO43, the rifampicin

derivative of the Indian isolate, BXO1 (Goel et al., 2002; Rajagopal et al., 1997). The bacteria visualised with the Atomic Force Microscope (AFM) showed spherical OMVs released into the surroundings by spontaneous blebbing (Figure 1a, b). Nanoparticle tracking analysis (NTA) revealed that the average diameter of the vesicles is about 125.8 +/- 1.6 nm (Figure 1c). When the *Xoo*-OMVs were imaged with the help of a Transmission electron microscope (TEM), they revealed that, like *Xcc*-OMVs (Bahar et al., 2016), *Xoo*-OMVs from BXO43 range from smaller vesicles (from 10-60 nm) to bigger vesicles (around 100-150 nm). The smaller and bigger vesicles are indicated by yellow and white arrowheads, respectively (Figure 1d).

Previous reports show that OMVs carry several toxins, virulence factors, PAMPs, and MAMPs that enable them to evoke an immune response in plants (Couto et al., 2015; Lappann et al., 2013; Lee et al., 2008). To identify the protein cargo carried by the *Xoo*-OMVs, we purified the crude *Xoo*-OMVs by density-gradient centrifugation and carried out a proteomic analysis. We precipitated the proteins isolated from the purified *Xoo*-OMVs with methanol-chloroform and subjected them to in-gel trypsin digestion. An ESI-MS/MS analysis of the digested peptides was carried out, and the proteins were identified by using Proteome Discoverer software (Thermo Fisher Scientific). The proteins identified from four biological replicate experiments, showing unique peptides ≥ 2, were represented in Table S1. We identified 290 proteins in the purified *Xoo*-OMVs. The identified proteins were grouped according to their subcellular localisation, predicted by PSortB software (Figure 1e). The biological and molecular functions of these proteins were designated using ShinyGO 0.82 software (Figure 1f, g). The gene ontology analysis revealed that the proteins are involved in localization, siderophore and iron transport, membrane organization and assembly (Figure 1f). The predicted molecular functions of the proteins suggested transmembrane transporter activity, catalytic activity, peptidase and cellulase activity, etc. (Figure 1g). Among the proteins identified from the purified *Xoo*-OMVs, the cytoplasmic proteins mostly comprised enzymes like, glnA, ace, ilvC, nerA, pepO, carB, etc. and minor fractions of chaperones, transcription factors, and ribosomal proteins (Table S1). Proteins localized in the outer membrane mostly consist of ion transporters (btuB, fyuA, bfeA, cirA, iroN), fimbrial proteins (pilQ, pilF), lipoproteins (vacJ, slp, rlpB, nlpB, pcp, etc.), outer membrane proteins (ompP1, ompW, ompA, etc) (Table 1).

We report that *Xoo*-OMVs, like *Xcc*-OMVs, carry known PAMPs like Ef-Tu, flagellar proteins (fliC, flgE, flgL, etc) and Ax21 (Bahar et al., 2016, 2014). *Xoo*-OMVs carry other virulence-associated proteins like regulator of pathogenicity factors (rpfN), adhesins (xadA), extracellular serine protease (*XOO*2375), and virulence protein (virK), etc. (Table 1). xadA helps in the invasion through hydathodes and is important for optimal virulence (Das et al., 2009). *XOO*2375 facilitates colonization through the xylem tissue (Mendes et al., 2016). We have also identified several plant-cell-wall-degrading enzymes, including cellulase (egl, *XOO*4036, *XOO*1077), endoglucanase (engXCA), esterase (estA), glucanase (celA), xylanase (xynA), etc. Several T6SS proteins (vgrG, hcp, *XOO*3480) and T4SS proteins, including pili-forming subunits (pilE, pilQ, pilF, pilJ, pilP, etc.), have also been identified from the purified *Xoo*-OMVs. Proteins involved in DSF processing, like fabF, oar protein, and ilvC, have also been identified in the *Xoo*-OMVs (Table 1).

Interestingly, *Xoo*-OMVs carry nine iron acquisition proteins, like TonB-dependent receptors (iroN, fyuA, btuB), iron transporters (fecA, yncD, CirA, etc) (Table 1). Identification of

Phosphate acquisition proteins like phoP, pstS, oprO, ppa, fruB in the purified *Xoo*-OMV proteome suggests the role of OMVs in nutrient acquisition (Table 1). Moreover, *Xoo*-OMVs carry several proteins that facilitate defense against host immune responses, particularly proteins involved in defense against ROS produced by the plants in response to OMVs, such as transaldolase, yojM, dps, organic hydroperoxide resistance protein (ohr), NADH-quinone oxidoreductase proteins (nuoF, nuoL, nuoG), etc. (Table 1). Overall, the protein content of the *Xoo*-OMVs suggests that the *Xoo*-OMVs can be involved in virulence, nutrient acquisition, invasion, colonization, and defense against the host's immune response.

2. *Xoo*-OMVs induce a Ca^{2+} signal in the elongation region of rice root

Ca^{2+} is one of the ubiquitous ions that play a key role in various cellular events in plants. Numerous reports describe the involvement of specific Ca^{2+} signals in sensing abiotic stimuli like heat stress, salt stress, and nutrient deficiency (Behera et al., 2017; Liao et al., 2017; Steinhorst et al., 2022). In the case of biotic stress responses, PAMPS like EF Tu, chitin, and flg22 induce a Ca^{2+} signal in plant cells (Cao et al., 2017; Keinath et al., 2015; Ranf et al., 2014). It is known that OMVs released by the pathogenic Gram-negative bacteria can facilitate infection and trigger an immune response in the host (Ellis and Kuehn, 2010). The early events that bring about such an immune response in the host plant are largely unexplored. We examined whether *Xoo*-OMVs induce any Ca^{2+} signal in plant cells at all. To accomplish this, we have used a Ca^{2+}-indicator stain, Calcium Green 1, AM, to stain CR 800 (resistant variety) and Khitish (susceptible variety) seedlings, respectively. Rice leaves are hydrophobic and difficult to stain; as an alternative, we imaged the roots. Rice roots are the entry point for *Xoo*-infection through contaminated irrigation water and soil (Naqvi, 2019). Furthermore, *Xoo* inoculated in the rice leaves could spread to the root (Ritbamrung et al., 2025). We stained the Khitish and CR 800 roots (n=6) with Calcium Green 1, AM (15 µM), the Ca^{2+}-sensitive dye, for 30 minutes as described in the materials and methods. After 5 minutes of incubation in the imaging solution,150 µl of *Xoo*-OMVs was added into the chamber of the slide. Images of the rice root tip were captured for 30 minutes at an interval of 1 minute. We observed an increase in Ca^{2+} concentration (depicted by the false colour code) after *Xoo*-OMV treatment (Figure 2a, b). The increase in Ca^{2+} concentration was observed in the epidermal cells of the zone of elongation of the rice root (Figure 2a, b). To analyze the change in Ca^{2+} concentration, we defined regions of interest (ROIs) on the epidermal cells in the distal elongation zone. We measured the fluorescent intensity in these ROIs for each rice seedling for the control set and for the seedlings treated with *Xoo*-OMVs and plotted them in the histogram for comparison (Figure 2c, d). Interestingly, both rice varieties exhibited an increase in Ca^{2+} concentration after 10 minutes of *Xoo*-OMVs application (Figure 2c, d). The change in Ca^{2+} concentration after *Xoo*-OMV application in the resistant variety (CR 800) and the susceptible variety (Khitish) was similar (Figure 2c, d).

To investigate whether *Xoo*-OMVs can induce an immune response in rice, we submerged 7-day-old Khitish and CR 800 seedlings in *Xoo*-OMVs for one hour. After that, the seedlings were incubated in sterile deionized water for another hour. It was observed that the resistant variety of rice, CR 800, could exhibit an Xa21-mediated immune response after the treatment as mentioned earlier, indicated by a three-fold elevation in the expression of *PR10b* compared

to the incubation in sterile water for 2 hours. On the other hand, Khitish, the susceptible variety of rice, could not mount any such immune response after exposure to *Xoo*-OMVs (Figure 2e). We further examined if CR 800 displayed an immune response against *Xoo*-OMVs in a Ca^{2+}-deprived condition. 7-day-old CR 800 and Khitish seedlings were pre-treated for 30 minutes with BAPTA-AM (25 μM), a cytosolic Ca^{2+}-chelator, and EGTA (2 mM), an extracellular Ca^{2+}-chelator, respectively. We observed that CR 800 did not display a significant immune response to *Xoo*-OMVs after pre-treatment with BAPTA-AM or EGTA, indicated by the reduced expression of PR10b (Figure 2e). These results point towards a Ca^{2+}-dependent immune response against *Xoo*-OMVs by rice.

3. *Xoo-OMVs* instigate rapid nanodomain enrichment in rice root and leaf plasma membrane in a Ca^{2+}-dependent manner

Nanodomains are highly ordered phases of the plant plasma membrane, which serve as functional congregations of several receptors and other membrane-associated proteins (Jaillais and Ott, 2020). It has been reported that the fusion of *Xcc*-OMVs with the plasma membrane of Arabidopsis leads to an increase in the order of the membrane (Tran et al., 2022). We have used Di-4-ANEPPDHQ, a polarity-sensitive membrane dye (Owen et al., 2012), to assess the state of lipid order of rice plasma membrane in the presence of *Xoo*-OMVs. Di-4-ANEPPDHQ shows a spectral shift of 60 nm between disordered and ordered phases of the membrane. The lipid order of the membrane can be quantified by using the generalized polarity (GP) values, ranging from -1 to +1, which indicate the polarity of the membrane, thereby suggesting the order of the membrane. Higher GP values correspond to a highly ordered or nanodomain-rich membrane (Owen et al., 2012).

We found that after 30 minutes of incubation in *Xoo*-OMVs, the roots of 7-day-old Khitish and CR 800 seedlings manifested a significant increase in the GP value of the plasma membrane ($P \leq 0.0001$, $n>6$), in contrast to the roots incubated in sterile water (control) (Figure 3a, b). The higher GP value indicated a highly ordered or a more nanodomain-enriched membrane (Figure 3b). We then investigated the duration for which the ordered state of the membrane was maintained. The roots were submerged in *Xoo*-OMVs for 60 and 90 minutes, respectively, and then stained with Di-4-ANEPPDHQ (3.5 μM). When visualized under a confocal microscope, the roots showed a significant elevation in the lipid order of the plasma membrane compared to those incubated in sterile water, at both time points (Figure S1c). We enquired if the Ca^{2+} signal in response to the *Xoo*-OMVs in plants is crucial for the nanodomain enrichment in the host plasma membrane. 7-day-old Khitish and CR 800 seedlings were pre-treated with EGTA (2 mM), and BAPTA-AM (25 μM) for 30 minutes. We found that in both varieties, the Ca^{2+}-chelated roots did not show a significant increase in the membrane order after 30 minutes of incubation in *Xoo*-OMVs (Figure 3a, b). These evidences suggest that the rapid nanodomain enrichment in the host membrane after exposure to *Xoo*-OMVs is Ca^{2+}-dependent.

We also examined whether *Xoo*-OMVs could lead to the rise of the lipid order in the plasma membrane of the leaf tissue. As it was difficult to stain rice leaves due to their hydrophobic nature, we isolated protoplasts from Khitish and CR 800 leaves and incubated the protoplasts with *Xoo*-OMVs for 30 minutes. The protoplasts were then stained with Di-4-ANEPPDHQ (3.5 μM) and mounted on a chambered slide for visualization. As the cell wall is essential in

maintaining plasma membrane protein mobility (Hosy et al., 2015) and regulating the size and stability of nanodomain (Daněk et al., 2020; McKenna et al., 2019), the protoplasts, due to the lack of a cell wall, show a wider range of lipid order than the roots. Nevertheless, the plasma membrane displayed a significant elevation in the lipid order after incubation with the *Xoo*-OMVs compared to the protoplasts incubated with sterile water (control) (Figure 3c). Similar to the rice roots, leaf protoplasts also displayed a compromised increase in the lipid order of the plasma membrane after Ca^{2+} chelation with BAPTA-AM (25 μM) (Figure 3c, d).
In order to verify that the rise of the lipid order of the host membrane is due to nanodomain enrichment during *Xoo*-OMV perception, we treated the rice leaf protoplasts with MβCD (2 mM), a sterol-depleting agent. As sterol is important for nanodomain congregation, protoplasts pre-treated with MβCD showed no increase in lipid order even upon incubation in *Xoo*-OMVs for 30 minutes (Figure 3c). The GP values (+1 to -1) of the respective experiments (n>6) have been plotted in a box plot, and their statistical differences have been calculated using one-way ANOVA with the help of GraphPad Prism software (Figure 3b, d).

4. Incorporation of *Xoo*-OMVs in the rice root and leaf plasma membrane is Ca^{2+}-dependent and mediated by nanodomain enrichment

OMVs are known to enter animal cells and deliver their cargo of virulence factors, enzymes, DNA, toxins, etc. (Bitto et al., 2017; Bomberger et al., 2009; O'Donoghue and Krachler, 2016). It is known that OMVs can enter the non-phagocytic host cells through various pathways, especially in a cholesterol-dependent lipid raft-mediated way (Kaparakis-Liaskos and Ferrero, 2015; Schaar et al., 2011). In Arabidopsis, *Xcc*-OMVs get incorporated into the plasma membrane in a sterol-dependent manner (Tran et al., 2022).
Similar to the aforementioned paper, we used FM4-64, a lipophilic dye, to stain the *Xoo*-OMVs in order to be able to track them. *Xoo*-OMVs or sterile water (control), were incubated with 1.5 mM FM4-64 for 10 minutes in the dark. After staining, both the stained *Xoo*-OMVs and sterile water (used as a control for fluorescence observed due to residual dye) were ultracentrifuged to eliminate the excess dye. The supernatant carrying the unbound dye was carefully discarded, keeping the pellet containing FM4-64-stained *Xoo*-OMVs intact. As sterile water lacks any lipid moiety to which FM4-64 can bind, no pellet is found in the control set. Sterile water was added to both tubes in an equal amount. The fluorescence of FM4-64 was checked through confocal laser scanning microscopy to visualize the localization of FM4-64-*Xoo*-OMVs in the plant tissue (Figure S2a).

Roots of 7-day-old Khitish and CR 800 seedlings (n>7) were incubated in FM4-64-*Xoo*-OMVs and the control treatment. It was observed that after 30 minutes of incubation in FM4-64-*Xoo*-OMVs, the plasma membrane of rice roots showed minimal fluorescence, indicating the initial stages of fusion of *Xoo*-OMVs with the rice membrane. After 60 minutes and 90 minutes of incubation, the fluorescence in the roots incubated in FM4-64-*Xoo*-OMVs increased considerably, indicating the incorporation of *Xoo*-OMVs into the rice root plasma membrane. No fluorescence was observed in the plasma membrane of the rice roots incubated in the control treatment, confirming that the remnant dye was insignificant (Figure S2c). Interestingly, we observed that the incorporation of the *Xoo*-OMVs occurs significantly more in Khitish roots (susceptible variety) than in CR 800 roots (resistant variety) (Figure 4e). This observation

suggests that the insertion of *Xoo*-OMVs into the rice membrane might play a key role in the perception of *Xoo*-OMVs and the following pathogenesis.

The fluorescence detection range of FM4-64 is close to that of chloroplasts. Thus, to visualize the membrane of the leaf tissues clearly without any chance of misinterpretation due to the autofluorescence of the chloroplasts, we used protoplasts isolated from the rice leaf tissues as the system for this experiment. Protoplasts, isolated from the leaves of Khitish and CR 800, were incubated with either FM4-64-*Xoo*-OMVs or the control treatment. The protoplasts that distinctly showed the plasma membrane were chosen for analysis. The ROIs was selected from the bright field images on the regions showing the plasma membrane (Figure S2b). It was noticed that the stained *Xoo*-OMVs were incorporated into the plasma membrane of the protoplasts after 60 minutes of incubation, like in the root (Figure 4c).

We further checked whether the Ca^{2+} signal in the host and the subsequent increase in lipid order of the host membrane play any role in the incorporation of *Xoo*-OMVs into the rice plasma membrane. On chelation of intracellular Ca^{2+} with BAPTA-AM (25 μM), the insertion of *Xoo*-OMVs in the rice root plasma membrane was significantly reduced (Figure 4a, b). Roots of Khitish and CR 800 seedlings were pre-treated with MβCD (2 mM) for 30 minutes to inhibit nanodomain formation. We found that, on sterol depletion from the membrane of rice roots, the fusion of *Xoo*-OMVs with the rice plasma membrane was diminished (Figure 4a, b). This indicated that insertion of the *Xoo*-OMVs into rice plasma membrane is a nanodomain-mediated process. Protoplasts isolated from the leaf tissues of Khitish and -CR 800 were pre-treated with MβCD (2 mM) and BAPTA-AM (25 μM) for 30 minutes. The pre-treated protoplasts manifested a significant decrease in the insertion of *Xoo*-OMVs into the rice plasma membrane (Figure 4c, d). Taken together, the results reveal that the integration of *Xoo*-OMVs into the plasma membrane of rice is a Ca^{2+}-dependent and nanodomain-mediated process.

Discussion:

We have endeavoured to understand the mechanism of perception of bacterial OMVs by the plants during host-pathogen interaction. We have performed a proteomic profiling of purified *Xoo*-OMVs and found several MAMPs, virulence-associated proteins, secretory system proteins, DSF-processing enzymes, and hydrolytic enzymes, which indicate the role of *Xoo*-OMVs during invasion and pathogenesis inside the host (Table 1). The presence of several cell-wall-degrading enzymes like cellulase, endoglucanase, esterase, etc., in the *Xoo*-OMV cargo (Table 1) is in accordance with the report that OMVs act as alternative machinery for the delivery of T2SS proteins, which are essential for virulence (Jha et al., 2007; Solé et al., 2015). According to prior reports, low iron conditions weaken the virulence of *Xoo*, advocating that iron is important for optimum virulence (Chatterjee et al., 2003; Subramoni et al., 2012). Nine iron-acquisition proteins are identified from the *Xoo*-OMVs, proposing the role of OMVs in adaptation and survival inside the host (Table 1). Intriguingly, we have found that *Xoo*-OMVs carry proteins to defend themselves against this ROS response, supported by a very recent study (Deng et al., 2025) (Table 1). The proteins carried by the *Xoo*-OMVs reflect the role of OMVs in plant-pathogen interaction.

MAMPs like flg22, elf18, etc., are known to induce Ca^{2+} signals in Arabidopsis (Ranf et al., 2014). The presence of such MAMPs and other immunogenic proteins in the *Xoo*-OMVs

interested us in investigating whether *Xoo*-OMVs can induce Ca^{2+} signals in rice or not. Our results demonstrate that exposure to *Xoo*-OMVs enhances cellular Ca^{2+} level in both CR 800 and Khitish roots after 10 minutes (Figure 2a, b). However, the Ca^{2+} signals we have observed are not specific to any particular MAMP; rather, it is a response of the root cells towards a mixture of MAMPs. Our results establish that, similar to the ROS burst (Bahar et al., 2016; Tran et al., 2022), the increase in the Ca^{2+} level is another hallmark of OMV perception by the plant.

It is well-established that plant pathogen-derived OMVs can trigger an immune response in the host plant (Bahar et al., 2016; Chalupowicz et al., 2023; McMillan et al., 2021). We have found that in the resistant variety CR 800, which expresses the *Xa21* gene (Mohapatra et al., 2023), *Xoo*-OMVs induce a Ca^{2+}-dependent Xa21–mediated immune response after just one hour of incubation. This denotes that the Ca^{2+} signal in rice is a key player in activating the immune response against *Xoo*-OMVs. The susceptible variety, Khitish, fails to evoke any such immune response. Our findings are consistent with previous reports (Liu et al., 2020; Thomas et al., 2016), where the resistant rice line, expressing *Xa21*, shows elevation in the expression of *PR10b* while the susceptible rice line does not.

Tran et al., 2020, showed that *Xcc*-OMVs can induce nanodomain enrichment in Arabidopsis plasma membrane. We have noticed that *Xoo*-OMVs could significantly elevate the lipid order of the CR 800 and Khitish roots and leaf protoplasts after 30 minutes of incubation in a Ca^{2+}-dependent manner (Figure 3). Additionally, we have established that *Xoo*-OMVs get incorporated into the plasma membrane of rice in a Ca^{2+}-dependent, sterol-mediated pathway (Figure 4). It was shown earlier that in Arabidopsis, the *Xcc*-OMVs get incorporated into the plasma membrane within 10 minutes (Tran et al., 2022). However, our data demonstrate that the incorporation of the *Xoo*-OMVs takes about 60 minutes in the rice plasma membrane (Figure S4b, c). The delay in the incorporation of the *Xoo*-OMVs is probably due to the differential composition of the cell walls between rice and Arabidopsis, as rice roots are more densely packed and rigid than Arabidopsis roots (Vogel, 2008). These findings imply that *Xoo*-OMVs trigger a Ca^{2+} signal in rice that leads to nanodomain enrichment, which is crucial for the following insertion of *Xoo*-OMVs in the rice plasma membrane.

Taken together, our outcomes reveal that *Xoo* releases OMVs, which contain abundant proteins, including MAMPs and virulence-associated proteins (Figure 1, Table 1). These MAMP-loaded *Xoo*-OMVs are recognized by the plants via a Ca^{2+} signal generation. The Ca^{2+} signal enables the organization of a nanodomain-enriched membrane by an unknown mechanism. We observed that this manner of OMV perception by Ca^{2+}-dependent nanodomain potentiation is similar in both resistant and susceptible varieties of rice. The nanodomain congregation is necessary to prepare the cell for a subsequent response reaction to combat the pathogenic challenge by aggregating the defence-related proteins into signalling hubs (Ott, 2017). These early events during the perception of *Xoo*-OMVs by the rice cell triggers a cascade of signalling. It provokes an immune response in the resistant variety of rice, CR 800, as CR 800 carries three R genes, *Xa21*, *xa13* and *xa5* (Mohapatra et al., 2023). After the initial perception of the OMVs, the R genes and other associated proteins activate an immune response to help prevent the infection. In the case of Khitish, the susceptible variety of rice, the

events following the perception of *Xoo*-OMVs fail to induce any immune response due to the absence of appropriate R genes and the associated repertoire of proteins. Therefore, our work depicts the mechanism of perception of *Xoo*-OMVs by rice through Ca^{2+} signalling (Figure 5). After the perception of the possible threat, the plants respond according to their genetic composition (presence or absence of R genes) to either resist the infection or be susceptible to it. In the Ca^{2+}-chelated condition, as the nanodomain enrichment is impaired, the insertion of *Xoo*-OMVs and the downstream immune response are all compromised. Our findings elucidate that the nanodomains are developed in a Ca^{2+}-dependent manner in rice plasma membrane during OMV perception. This is the first report of the involvement of Ca^{2+} in plant nanodomain enrichment with respect to plant-bacteria interaction. It is proposed that putative Ca^{2+} channels present in the plasma membrane nanodomain get activated after perception of a specific stimulus and generate a Ca^{2+} signal that is further decoded by various Ca^{2+}-binding proteins (Hdedeh et al., 2025). Interestingly, our finding suggests that Ca^{2+} is involved in the nanodomain enrichment, which is a prerequisite for biotic and abiotic stress response in plants. Exploring the mechanism of Ca^{2+}-mediated nanodomain configuration would be of great interest in understanding the recruitment of the various signalling components. It would be of utmost importance to study the ubiquitous role played by Ca^{2+} signals in both the formation of stimulus-specific nanodomain and the decoding of the nanodomain-mediated signals.

Materials and methods:

Plant and bacterial samples:

Khitish and CR 800 (*Oryza sativa subsp. indica*) were grown hydroponically at 30 ºC under a 16-hour light / 8-hour dark condition, with 70-80 % humidity. *Xanthomonas oryzae pv. oryzae* strain BXO43 was grown in peptone sucrose (PS) media with rifampicin (50 µg/ml) for 2 days at 28 ºC.

Isolation of outer membrane vesicles:

A bacterial culture of BXO43 was grown to O.D. 0.6-0.8 at 650nm in PSA media with rifampicin (50 µg/ml) at 28 ºC with shaking at 200 rpm. *Xoo*-OMVs were isolated according to the protocol of Mordukhovich and Bahar, 2017. Briefly, the culture was pelleted at 10,000g for 30 minutes, and the supernatant was filtered through a 0.45µm syringe filter. The filtered cell-free supernatant was subjected to ultracentrifugation at the speed of 100000g at 4 ºC for 2 hours. The resulting pellet was dissolved in sterile deionized water and filtered through a 0.22 µm filter before centrifugation at 170000g at 4 ºC for 2 hours. The *Xoo*-OMVs were purified through density gradient centrifugation using OptiPrep diluent buffer (Sigma) following the protocol described in Mordukhovich and Bahar, 2017. The resultant pellet was weighed and re-suspended in sterile deionized water or in Ca^{2+} imaging buffer (for Ca^{2+} imaging) at a concentration of 100 mg/ml. Isolated *Xoo*-OMVs were stored at 4 ºC and utilized within 3 days of isolation. The total protein content of the *Xoo*-OMVs was quantified using Bradford assay (Biorad).

Nanoparticle Tracking Analysis (NTA):

The hydrodynamic size range of the *Xoo*-OMVs was observed through Nanoparticle Tracking Analysis (NTA). The *Xoo*-OMVs were diluted 200 times in sterile water and injected into the laser chamber of Nanosight NS300. The videos were analysed and plotted in a graph through the software of NTA 3.2 Dev Build 3.2.16., (n=3).

Atomic force microscopy (AFM):

Atomic force microscopy (AFM) was performed with the *Xanthomonas oryzae pv. oryzae* bacteria to visualize the spontaneous production of OMVs. *Xoo* cells were diluted with PBS to an O.D. of 0.2. The diluted *Xoo* cells were incubated at 28 ^{o}C for 1 hour. 3 µl of the cells were dropped on a freshly cleaved mica sheet. The sheet was dried inside a vacuum desiccator for 1 hour and visualized with the help of the AFM-MFP-3D (Oxford Instruments) in tapping mode.

Transmission electron microscopy (TEM):

Xoo-OMVs were fixed in 2 % glutaraldehyde, and 5µl of the sample was dropped on a copper grid. The sample was stained with 1% uranyl acetate and visualized under a Jeol-JEM-2100 Plus transmission electron microscope.

SDS-PAGE:

Xoo-OMV sample was added to water: methanol: chloroform=4:3:1 and vortexed for 5 minutes, followed by centrifugation at 14000g at 4 ^{o}C for 5 minutes. The protein pellet was recovered from the interface of the aqueous and organic phases. To the pellet, 300 µl of methanol was added and vortexed again, followed by centrifugation. The resulting protein pellet was dried and dissolved in 1X Tris-glycine sample loading buffer (Invitrogen) and heated at 95 ^{o}C for 10 minutes. The precipitated protein sample was run in 12 % SDS-PAGE and stained with Coomassie blue G-250 overnight for analysis by LC-ESI-MS/MS.

In-gel trypsin digestion

The in-gel trypsin digestion was performed according to (Sidhu et al., 2008), with the exception that formic acid was used instead of TFA for better ionization. Briefly, the protein sample was run in the gel shortly, to prevent the bands from resolving fully. The compressed protein band consisting of all the proteins was cut and de-stained with ACN and ammonium bicarbonate. The proteins were digested with trypsin for 15 minutes, followed by protein extraction for 24 hours. An additional step of 1 hour of protein extraction was carried out in order to maximize the peptide concentration. The peptides were lyophilized and stored at -20 ^{o}C until further analysis through the ESI-MS/MS system.

LC-ESI-MS/MS of digested peptides:

The digested peptides were reconstituted in 10 µl of 1 % formic acid and run in an Orbitrap Fusion Lumos mass spectrometer (Thermo Fisher Scientific). 0.75 µg of peptides were subjected to the nano-flow (75 µm x 500 mm, EASY-Spray™ PepMap™ Neo C18 column, with 100 Å pore size) and run for 140 minutes. The system was run with Solvent A = 0.1% formic acid and Solvent B = 80 % ACN 0.1 % formic acid. The peptides were eluted at a

constant flow of 0.3 µl/min, starting with 5 % solvent B to 75 % solvent B upto 125 minutes, then decreasing to 5 % solvent B until 140 minutes. The scan was performed in a data-dependent mode with 20 dependent scans with a resolution of 60000 with a scan range of m/z from 350-2000. The peaks of the significant proteins were plotted directly using X-calibur software™ (Thermo Fisher Scientific). The proteins were identified using the Proteome Discoverer software. Percolator function was used along with Sequest HT for better identification of the proteins. The following parameters were selected for protein identification: enzyme: trypsin; missed cleavage: 2; precursor mass tolerance 10 ppm; peptide charge +1, +2 and +3; ion type: monoisotopic. The reference proteome of *Xanthomonas oryzae pv. oryzae* (strain KACC10331 / KXO85) (Taxon ID. 291331), available in the Uniprot database was used to compare and recognize the proteins. 4 independent LC-ESI-MS/MS experiments were conducted using separate protein preparations from 4 different batches of culture.

The subcellular localization of the proteins was identified using the PSORTb v.3.0 software. The gene ontology of the identified proteins was designated by using the ShinyGo 0.82 software. Utilizing this software, the proteins were assembled into respective groups defining their biological and molecular function.

Calcium Green 1, AM staining of rice seedlings:

7-day-old Khitish and CR 800 seedlings (n=5) were stained with Calcium Green1, AM, (Invitrogen) in the presence of an eserine, phytostigmine salicylate (0.5 mg/ml) (Sigma) for better loading of the dye. For visualization, the stained rice roots were kept inside chambered slides and covered by an agar block to prevent any movement. 75 µl of sterile water was added to keep the roots moist while imaging. The roots were visualized under a Zeiss LSM800 confocal laser scanning microscope. The roots were excited at the wavelength of 488 nm at an interval of 1 minute under a PLAN APO 10X dry objective with a 0.5X magnification, and emission was collected in the range of 500-600 nm. After 5 minutes of imaging 150 µl of *Xoo*-OMVs (100mg/ml) were added to the chambered slide. The images were analyzed using the ImageJ Fiji software. The epidermis region of the elongation zone was selected as the region of interest (ROI). The fluorescence intensity values were background corrected and normalized with the baseline average intensity to obtain $\Delta F/F$. The $\Delta F/F$ values of seedlings treated with sterile water and *Xoo*-OMVs, respectively, at an interval of 5 minutes were plotted in a histogram using GraphPad Prism software. The intensity values of the *Xoo*-OMVs treatment and the control at each time point were compared using two-way ANOVA. The statistical difference is shown as, ns, not significant, $*P \leq 0.05$; $**P \leq 0.01$, $***P \leq 0.001$, $****P \leq 0.0001$.

qRT-PCR:

Immune response in rice after exposure to *Xoo*-OMVs was examined via qRT-PCR. 10-day-old Khitish and CR 800 seedlings were incubated in *Xoo*-OMVs for 1 hour, followed by an hour of incubation in sterile water. For Ca^{2+} chelation, the rice roots were pre-treated with 25 µM BAPTA-AM (Invitrogen) and 2 mM EGTA (Cayman) for 30 minutes, followed by incubation in *Xoo*-OMVs for 1 hour in the presence of BAPTA-AM and EGTA, respectively. Then the seedlings were incubated in sterile water for an hour. For the control treatment, the

rice roots were incubated in sterile water for 2 hours. Three independent replicates of the experiments had been performed with each replicate consisting of 5 seedlings. RNA was isolated from the root tissue of the rice seedlings of each independent replicate, with subsequent cDNA preparation. qRT PCR was performed to inspect the expression of *PR10b* gene with the following primers: qActin-F (5′ ATCCTTGTATGCTAGCGGTCGA-3′), qActin-R (5′-ATCCAACCGGAGGATAGCATG-3′); PR10b-F (5′-TGTGGAAGGTCTGCTTGGAC-3′), PR10b-R (5′-CCTTTAGCACGTGAGTTGCG-3′) (Liu et al., 2020).

Quantification of plasma membrane lipid order:

7-day-old Khitish and CR 800 seedlings (n>6) and protoplasts, collected from the leaf tissues, were analyzed for lipid order quantification assay. The *Xoo*-OMVs were diluted with sterile water to a concentration of 25 mg/ml, and rice roots were incubated in it for 30 minutes, 1 hour, and 1.5 hours, respectively. The protoplasts were subjected to incubation with the *Xoo*-OMV for 30 minutes. The seedlings and protoplasts were incubated in sterile water as the control. The roots and protoplasts were pre-treated with BAPTA-AM (25 μM) (Invitrogen), EGTA (2 mM) (Cayman), and MβCD (2 mM) (Sigma), respectively, for 30 minutes during appropriate experiments. The roots and protoplasts were stained with 4 μM Di-4-ANEPPDHQ for 10 minutes. The roots and protoplasts were viewed under a HC PL APO CS 60X oil immersion objective according to the protocol described in Owen et al., 2012. Briefly, the sample was excited at 488 nm, and emission was collected at two different ranges from 500-580 nm (ordered phase) and 620-750 nm (disordered phase). The GP values (+1 to -1) were plotted in a box plot.

Fusion assay of OMV with FM4-64:

Xoo-OMVs were stained with 1.5mM FM4-64 (Invitrogen) for 10 minutes on ice in the dark. Stained *Xoo*-OMVs were subjected to ultracentrifugation at 170000g at 4ºC for 1 hour to remove the residual stain. The *Xoo*-OMV pellet was resuspended in sterile water to the concentration of 25mg/ml, then kept at 4ºC, and used within 2 days. The stain was added to sterile water and incubated on ice in the dark for 10 minutes. It was ultracentrifuged, and the supernatant was discarded. Sterile water was added to the tube; this was used as the mock treatment. 7-day-old Khitish and CR 800 seedlings (n>7), and leaf protoplasts were incubated with stained *Xoo*-OMVs and the mock treatment for 30 minutes, 1 hour, and 1.5 hours, respectively. The seedlings were imaged under Leica SP8 STED confocal laser scanning microscope under a HC PL APO CS 60X oil immersion objective. FM4-64 was excited at 568 nm, and emission was collected from 700-795 nm. For Ca^{2+} chelation, the seedlings were pre-treated with BAPTA-AM (25 μM) (Invitrogen) and EGTA (2 mM) (Cayman), respectively, for 30 minutes. Pretreatment with MβCD (2 mM) (Sigma) for 30 minutes was carried out for sterol depletion.

Statistical analysis:

The confocal microscope images were analyzed using ImageJ software to obtain the fluorescence intensity values and GP values. For the lipid order and fusion assay, 15 ROIs were selected from each image taken of individual seedlings. The graphs, including the histograms, box plots, and line curves, with these values were plotted with the help of the GraphPad Prism

software. The statistical analysis was carried out using the GraphPad Prism software. One-way ANOVA was used to deduce the statistical difference between the samples unless specified. The p-value was taken as 0.05 with ns, not significant, *P ≤ 0.05; **P ≤ 0.01, ***P ≤ 0.001, ****P ≤ 0.0001.

Author contributions:

SB conceptualized the project and arranged the funding. IM and SB designed the experiments. IM and HD performed the experiments. IM and SB analyzed the data. IM and SB wrote the manuscript.

Acknowledgments

This work was funded by the SRG/2022/002293 grant from the Department of Science and Technology, Government of India. We thank Dr. H. K. Patel from CSIR-CCMB for providing us with the *Xoo* strains that have been used in the study. We are thankful to the Rice Research Station, Chinsurah, West Bengal, for providing us with the seeds of Khitish and CR 800. We acknowledge the Central Instrumentation Facility (CIF) of CSIR-Indian Institute of Chemical Biology (CSIR-IICB). We are thankful to DBT-ILS for the TEM and ESI-MS/MS experiments. We acknowledge Mr. Sandip Barman for critically reading the manuscript for editing.

Conflict of interest

The authors declare that they have no conflicts of interest.

Supporting information:

Table S1: All the proteins isolated from *Xoo*-OMVs, arranged on the basis of subcellular localization.

Fig S1: Temporal nanodomain enrichment in rice roots after exposure to *Xoo*-OMVs in Ca^{2+}-chelated condition.

Fig S2: Purified *Xoo*-OMVs induce nanodomain enrichment in rice root plasma membrane.

Fig S3: Insertion of *Xoo*-OMVs into the plasma membrane of rice with respect to time.

References:

Ali, R., Ma, W., Lemtiri-Chlieh, F., Tsaltas, D., Leng, Q., Von Bodman, S., Berkowitz, G.A., 2007. Death Don't Have No Mercy and Neither Does Calcium: *Arabidopsis* CYCLIC NUCLEOTIDE GATED CHANNEL2 and Innate Immunity. Plant Cell 19, 1081–1095. https://doi.org/10.1105/tpc.106.045096

Altindis, E., Fu, Y., Mekalanos, J.J., 2014. Proteomic analysis of *Vibrio cholerae* outer membrane vesicles. Proc. Natl. Acad. Sci. 111. https://doi.org/10.1073/pnas.1403683111

Bahar, O., Mordukhovich, G., Luu, D.D., Schwessinger, B., Daudi, A., Jehle, A.K., Felix, G., Ronald, P.C., 2016. Bacterial Outer Membrane Vesicles Induce Plant Immune Responses. Mol. Plant-Microbe Interactions 29, 374–384. https://doi.org/10.1094/MPMI-12-15-0270-R

Bahar, O., Pruitt, R., Luu, D.D., Schwessinger, B., Daudi, A., Liu, F., Ruan, R., Fontaine-Bodin, L., Koebnik, R., Ronald, P., 2014. The *Xanthomonas* Ax21 protein is processed by the general secretory system and is secreted in association with outer membrane vesicles. PeerJ 2, e242. https://doi.org/10.7717/peerj.242

Behera, S., Long, Y., Schmitz-Thom, I., Wang, X., Zhang, C., Li, H., Steinhorst, L., Manishankar, P., Ren, X., Offenborn, J.N., Wu, W., Kudla, J., Wang, Y., 2017. Two spatially and temporally distinct Ca^{2+} signals convey *Arabidopsis thaliana* responses to K^{+} deficiency. New Phytol. 213, 739–750. https://doi.org/10.1111/nph.14145

Behera, S., Wang, N., Zhang, C., Schmitz-Thom, I., Strohkamp, S., Schültke, S., Hashimoto, K., Xiong, L., Kudla, J., 2015. Analyses of Ca^{2+} dynamics using a ubiquitin-10 promoter-driven Yellow Cameleon 3.6 indicator reveal reliable transgene expression and differences in cytoplasmic Ca^{2+} responses in Arabidopsis and rice (*Oryza sativa*) roots. New Phytol. 206, 751–760. https://doi.org/10.1111/nph.13250

Beveridge, T.J., 1999. Structures of gram-negative cell walls and their derived membrane vesicles. J. Bacteriol. 181, 4725–4733. https://doi.org/10.1128/JB.181.16.4725-4733.1999

Bitto, N.J., Chapman, R., Pidot, S., Costin, A., Lo, C., Choi, J., D'Cruze, T., Reynolds, E.C., Dashper, S.G., Turnbull, L., Whitchurch, C.B., Stinear, T.P., Stacey, K.J., Ferrero, R.L., 2017. Bacterial membrane vesicles transport their DNA cargo into host cells. Sci. Rep. 7, 7072. https://doi.org/10.1038/s41598-017-07288-4

Bomberger, J.M., MacEachran, D.P., Coutermarsh, B.A., Ye, S., O'Toole, G.A., Stanton, B.A., 2009. Long-Distance Delivery of Bacterial Virulence Factors by Pseudomonas aeruginosa Outer Membrane Vesicles. PLoS Pathog. 5, e1000382. https://doi.org/10.1371/journal.ppat.1000382

Bücherl, C.A., Jarsch, I.K., Schudoma, C., Segonzac, C., Mbengue, M., Robatzek, S., MacLean, D., Ott, T., Zipfel, C., 2017. Plant immune and growth receptors share common signalling components but localise to distinct plasma membrane nanodomains. eLife 6, e25114. https://doi.org/10.7554/eLife.25114

Buck, A.H., Coakley, G., Simbari, F., McSorley, H.J., Quintana, J.F., Le Bihan, T., Kumar, S., Abreu-Goodger, C., Lear, M., Harcus, Y., Ceroni, A., Babayan, S.A., Blaxter, M., Ivens, A., Maizels, R.M., 2014. Exosomes secreted by nematode parasites transfer small RNAs to mammalian cells and modulate innate immunity. Nat. Commun. 5, 5488. https://doi.org/10.1038/ncomms6488

Cao, X.-Q., Jiang, Z.-H., Yi, Y.-Y., Yang, Y., Ke, L.-P., Pei, Z.-M., Zhu, S., 2017. Biotic and Abiotic Stresses Activate Different Ca^{2+} Permeable Channels in Arabidopsis. Front. Plant Sci. 8. https://doi.org/10.3389/fpls.2017.00083

Chalupowicz, L., Mordukhovich, G., Assoline, N., Katsir, L., Sela, N., Bahar, O., 2023. Bacterial outer membrane vesicles induce a transcriptional shift in arabidopsis towards immune system activation leading to suppression of pathogen growth in planta. J. Extracell. Vesicles 12, 12285. https://doi.org/10.1002/jev2.12285

Chatterjee, S., Sankaranarayanan, R., Sonti, R.V., 2003. PhyA, a Secreted Protein of *Xanthomonas oryzae* pv. *oryzae*, Is Required for Optimum Virulence and Growth on Phytic Acid as a Sole Phosphate Source. Mol. Plant-Microbe Interactions 16, 973–982. https://doi.org/10.1094/MPMI.2003.16.11.973

Chen, D.J., Osterrieder, N., Metzger, S.M., Buckles, E., Doody, A.M., DeLisa, M.P., Putnam, D., 2010. Delivery of foreign antigens by engineered outer membrane vesicle vaccines. Proc. Natl. Acad. Sci. 107, 3099–3104. https://doi.org/10.1073/pnas.0805532107

Chowdhury, C., Jagannadham, M.V., 2013. Virulence factors are released in association with outer membrane vesicles of Pseudomonas syringae pv. tomato T1 during normal

growth. Biochim. Biophys. Acta BBA - Proteins Proteomics 1834, 231–239. https://doi.org/10.1016/j.bbapap.2012.09.015

Couto, N., Schooling, S.R., Dutcher, J.R., Barber, J., 2015. Proteome Profiles of Outer Membrane Vesicles and Extracellular Matrix of *Pseudomonas aeruginosa* Biofilms. J. Proteome Res. 14, 4207–4222. https://doi.org/10.1021/acs.jproteome.5b00312

Daněk, M., Angelini, J., Malínská, K., Andrejch, J., Amlerová, Z., Kocourková, D., Brouzdová, J., Valentová, O., Martinec, J., Petrášek, J., 2020. Cell wall contributes to the stability of plasma membrane nanodomain organization of *Arabidopsis thaliana* FLOTILLIN2 and HYPERSENSITIVE INDUCED REACTION1 proteins. Plant J. 101, 619–636. https://doi.org/10.1111/tpj.14566

Das, A., Rangaraj, N., Sonti, R.V., 2009. Multiple Adhesin-Like Functions of *Xanthomonas oryzae* pv. *oryzae* Are Involved in Promoting Leaf Attachment, Entry, and Virulence on Rice. Mol. Plant-Microbe Interactions® 22, 73–85. https://doi.org/10.1094/MPMI-22-1-0073

Deng, J., Li, W., Wang, Z., Zeng, J., Cai, Q., 2025. KatB, a bacterial extracellular vesicles (EVs)-secreted catalase, detoxifies reactive oxygen species (ROS) and promotes pathogen proliferation in plants. J. Integr. Plant Biol. jipb.13894. https://doi.org/10.1111/jipb.13894

Ellis, T.N., Kuehn, M.J., 2010. Virulence and Immunomodulatory Roles of Bacterial Outer Membrane Vesicles. Microbiol. Mol. Biol. Rev. 74, 81–94. https://doi.org/10.1128/MMBR.00031-09

Feitosa-Junior, O.R., Stefanello, E., Zaini, P.A., Nascimento, R., Pierry, P.M., Dandekar, A.M., Lindow, S.E., Da Silva, A.M., 2019. Proteomic and Metabolomic Analyses of *Xylella fastidiosa* OMV-Enriched Fractions Reveal Association with Virulence Factors and Signalling Molecules of the DSF Family. Phytopathology® 109, 1344–1353. https://doi.org/10.1094/PHYTO-03-19-0083-R

Fernandez-Calvino, L., Faulkner, C., Walshaw, J., Saalbach, G., Bayer, E., Benitez-Alfonso, Y., Maule, A., 2011. Arabidopsis Plasmodesmal Proteome. PLoS ONE 6, e18880. https://doi.org/10.1371/journal.pone.0018880

Goel, A.K., Rajagopal, L., Nagesh, N., Sonti, R.V., 2002. Genetic Locus Encoding Functions Involved in Biosynthesis and Outer Membrane Localization of Xanthomonadin in *Xanthomonas oryzae* pv. oryzae. J. Bacteriol. 184, 3539–3548. https://doi.org/10.1128/JB.184.13.3539-3548.2002

Grant, M., Brown, I., Adams, S., Knight, M., Ainslie, A., Mansfield, J., 2000. The *RPM1* plant disease resistance gene facilitates a rapid and sustained increase in cytosolic calcium that is necessary for the oxidative burst and hypersensitive cell death. Plant J. 23, 441–450. https://doi.org/10.1046/j.1365-313x.2000.00804.x

Gronnier, J., Crowet, J.-M., Habenstein, B., Nasir, M.N., Bayle, V., Hosy, E., Platre, M.P., Gouguet, P., Raffaele, S., Martinez, D., Grelard, A., Loquet, A., Simon-Plas, F., Gerbeau-Pissot, P., Der, C., Bayer, E.M., Jaillais, Y., Deleu, M., Germain, V., Lins, L., Mongrand, S., 2017. Structural basis for plant plasma membrane protein dynamics and organization into functional nanodomains. eLife 6, e26404. https://doi.org/10.7554/eLife.26404

Hdedeh, O., Mercier, C., Poitout, A., Martinière, A., Zelazny, E., 2025. Membrane nanodomains to shape plant cellular functions and signalling. New Phytol. 245, 1369–1385. https://doi.org/10.1111/nph.20367

Hosy, E., Martinière, A., Choquet, D., Maurel, C., Luu, D.-T., 2015. Super-Resolved and Dynamic Imaging of Membrane Proteins in Plant Cells Reveal Contrasting Kinetic Profiles and Multiple Confinement Mechanisms. Mol. Plant 8, 339–342. https://doi.org/10.1016/j.molp.2014.10.006

Huang, Y., Zhu, F., Koh, J., Stanton, D., Chen, S., Wang, N., 2022. Proteomic and bioinformatic analyses of proteins in the outer membrane and extracellular compartments and outer membrane vesicles of Candidatus Liberibacter species. Front. Microbiol. 13, 977710. https://doi.org/10.3389/fmicb.2022.977710

Jaillais, Y., Ott, T., 2020. The Nanoscale Organization of the Plasma Membrane and Its Importance in Signalling: A Proteolipid Perspective. Plant Physiol. 182, 1682–1696. https://doi.org/10.1104/pp.19.01349

Jan, A.T., 2017. Outer Membrane Vesicles (OMVs) of Gram-negative Bacteria: A Perspective Update. Front. Microbiol. 8, 1053. https://doi.org/10.3389/fmicb.2017.01053

Jang, K.-S., Sweredoski, M.J., Graham, R.L.J., Hess, S., Clemons, W.M., 2014. Comprehensive proteomic profiling of outer membrane vesicles from Campylobacter jejuni. J. Proteomics 98, 90–98. https://doi.org/10.1016/j.jprot.2013.12.014

Jha, G., Rajeshwari, R., Sonti, R.V., 2007. Functional Interplay Between Two *Xanthomonas oryzae* pv. *oryzae* Secretion Systems in Modulating Virulence on Rice. Mol. Plant-Microbe Interactions® 20, 31–40. https://doi.org/10.1094/MPMI-20-0031

Kadurugamuwa, J.L., Beveridge, T.J., 1996. Bacteriolytic effect of membrane vesicles from Pseudomonas aeruginosa on other bacteria including pathogens: conceptually new antibiotics. J. Bacteriol. 178, 2767–2774. https://doi.org/10.1128/jb.178.10.2767-2774.1996

Kaparakis-Liaskos, M., Ferrero, R.L., 2015. Immune modulation by bacterial outer membrane vesicles. Nat. Rev. Immunol. 15, 375–387. https://doi.org/10.1038/nri3837

Keinath, N.F., Waadt, R., Brugman, R., Schroeder, J.I., Grossmann, G., Schumacher, K., Krebs, M., 2015. Live Cell Imaging with R-GECO1 Sheds Light on flg22- and Chitin-Induced Transient [Ca 2+] cyt Patterns in Arabidopsis. Mol. Plant 8, 1188–1200. https://doi.org/10.1016/j.molp.2015.05.006

Kulp, A., Kuehn, M.J., 2010. Biological Functions and Biogenesis of Secreted Bacterial Outer Membrane Vesicles. Annu. Rev. Microbiol. 64, 163–184. https://doi.org/10.1146/annurev.micro.091208.073413

Lappann, M., Otto, A., Becher, D., Vogel, U., 2013. Comparative Proteome Analysis of Spontaneous Outer Membrane Vesicles and Purified Outer Membranes of Neisseria meningitidis. J. Bacteriol. 195, 4425–4435. https://doi.org/10.1128/JB.00625-13

Lee, E., Bang, J.Y., Park, G.W., Choi, D., Kang, J.S., Kim, H., Park, K., Lee, J., Kim, Y., Kwon, K., Kim, K., Gho, Y.S., 2007. Global proteomic profiling of native outer membrane vesicles derived from ***Escherichia coli*** . PROTEOMICS 7, 3143–3153. https://doi.org/10.1002/pmic.200700196

Lee, E., Choi, D., Kim, K., Gho, Y.S., 2008. Proteomics in gram-negative bacterial outer membrane vesicles. Mass Spectrom. Rev. 27, 535–555. https://doi.org/10.1002/mas.20175

Legrand, A., G.-Cava, D., Jolivet, M.-D., Decossas, M., Lambert, O., Bayle, V., Jaillais, Y., Loquet, A., Germain, V., Boudsocq, M., Habenstein, B., Vélez Tirado, M., Mongrand, S., 2023. Structural determinants of REMORIN nanodomain formation in anionic membranes. Biophys. J. 122, 2192–2202. https://doi.org/10.1016/j.bpj.2022.12.035

Liao, C., Zheng, Y., Guo, Y., 2017. MYB30 transcription factor regulates oxidative and heat stress responses through ANNEXIN-mediated cytosolic calcium signalling in *Arabidopsis*. New Phytol. 216, 163–177. https://doi.org/10.1111/nph.14679

Liu, F., Zhang, W., Schwessinger, B., Wei, T., Ruan, D., Ronald, P., 2020. The Rice Xa3 Gene Confers Resistance to Xanthomonas oryzae pv. oryzae in the Model Rice Kitaake Genetic Background. Front. Plant Sci. 11, 49. https://doi.org/10.3389/fpls.2020.00049

Maphosa, S., Moleleki, L.N., 2021. Isolation and Characterization of Outer Membrane Vesicles of Pectobacterium brasiliense 1692. Microorganisms 9, 1918. https://doi.org/10.3390/microorganisms9091918

McBroom, A.J., Kuehn, M.J., 2007. Release of outer membrane vesicles by Gram-negative bacteria is a novel envelope stress response. Mol. Microbiol. 63, 545–558. https://doi.org/10.1111/j.1365-2958.2006.05522.x

McKenna, J.F., Rolfe, D.J., Webb, S.E.D., Tolmie, A.F., Botchway, S.W., Martin-Fernandez, M.L., Hawes, C., Runions, J., 2019. The cell wall regulates dynamics and size of plasma-membrane nanodomains in *Arabidopsis*. Proc. Natl. Acad. Sci. 116, 12857–12862. https://doi.org/10.1073/pnas.1819077116

McMillan, H.M., Kuehn, M.J., 2023. Proteomic Profiling Reveals Distinct Bacterial Extracellular Vesicle Subpopulations with Possibly Unique Functionality. Appl. Environ. Microbiol. 89, e01686-22. https://doi.org/10.1128/aem.01686-22

McMillan, H.M., Zebell, S.G., Ristaino, J.B., Dong, X., Kuehn, M.J., 2021. Protective plant immune responses are elicited by bacterial outer membrane vesicles. Cell Rep. 34, 108645. https://doi.org/10.1016/j.celrep.2020.108645

Mendes, J.S., Santiago, A.S., Toledo, M.A.S., Horta, M.A.C., De Souza, A.A., Tasic, L., De Souza, A.P., 2016. In vitro Determination of Extracellular Proteins from Xylella fastidiosa. Front. Microbiol. 7. https://doi.org/10.3389/fmicb.2016.02090

Mordukhovich, G., & Bahar, O., 2017. Isolation of outer membrane vesicles from phytopathogenic Xanthomonas campestris pv. campestris. BIO-protocol, *7*. https://doi.org/10.21769/BioProtoc.2160

Mohapatra, S., Barik, S.R., Dash, P.K., Lenka, D., Pradhan, K.C., Raj K. R, R., Mohanty, S.P., Mohanty, M.R., Sahoo, A., Jena, B.K., Panda, A.K., Panigrahi, D., Dash, S.K., Meher, J., Sahoo, C.R., Mukherjee, A.K., Das, L., Behera, L., Pradhan, S.K., 2023. Molecular Breeding for Incorporation of Submergence Tolerance and Durable Bacterial Blight Resistance into the Popular Rice Variety 'Ranidhan.' Biomolecules 13, 198. https://doi.org/10.3390/biom13020198

Nagano, M., Ishikawa, T., Fujiwara, M., Fukao, Y., Kawano, Y., Kawai-Yamada, M., Shimamoto, K., 2016. Plasma Membrane Microdomains Are Essential for Rac1-RbohB/H-Mediated Immunity in Rice. Plant Cell 28, 1966–1983. https://doi.org/10.1105/tpc.16.00201

Niño-Liu, D.O., Ronald, P.C., Bogdanove, A.J., 2006. *Xanthomonas oryzae* pathovars: model pathogens of a model crop. Mol. Plant Pathol. 7, 303–324. https://doi.org/10.1111/j.1364-3703.2006.00344.x

O'Donoghue, E.J., Krachler, A.M., 2016. Mechanisms of outer membrane vesicle entry into host cells: MicroReview - OMV entry into host cells. Cell. Microbiol. 18, 1508–1517. https://doi.org/10.1111/cmi.12655

Ott, T., 2017. Membrane nanodomains and microdomains in plant–microbe interactions. Curr. Opin. Plant Biol. 40, 82–88. https://doi.org/10.1016/j.pbi.2017.08.008

Owen, D.M., Rentero, C., Magenau, A., Abu-Siniyeh, A., Gaus, K., 2012. Quantitative imaging of membrane lipid order in cells and organisms. Nat. Protoc. 7, 24–35. https://doi.org/10.1038/nprot.2011.419

Perraki, A., Gronnier, J., Gouguet, P., Boudsocq, M., Deroubaix, A.-F., Simon, V., German-Retana, S., Legrand, A., Habenstein, B., Zipfel, C., Bayer, E., Mongrand, S., Germain, V., 2018. REM1.3's phospho-status defines its plasma membrane nanodomain organization and activity in restricting PVX cell-to-cell movement. PLOS Pathog. 14, e1007378. https://doi.org/10.1371/journal.ppat.1007378

Rajagopal, L., Sundari, C.S., Balasubramanian, D., Sonti, R.V., 1997. The bacterial pigment xanthomonadin offers protection against photodamage. FEBS Lett. 415, 125–128. https://doi.org/10.1016/S0014-5793(97)01109-5

Ranf, S., 2017. Sensing of molecular patterns through cell surface immune receptors. Curr. Opin. Plant Biol. 38, 68–77. https://doi.org/10.1016/j.pbi.2017.04.011

Ranf, S., Eschen-Lippold, L., Fröhlich, K., Westphal, L., Scheel, D., Lee, J., 2014. Microbe-associated molecular pattern-induced calcium signalling requires the receptor-like cytoplasmic kinases, PBL1 and BIK1. BMC Plant Biol. 14, 374. https://doi.org/10.1186/s12870-014-0374-4

Ranf, S., Eschen-Lippold, L., Pecher, P., Lee, J., Scheel, D., 2011. Interplay between calcium signalling and early signalling elements during defence responses to microbe- or damage-associated molecular patterns. Plant J. 68, 100–113. https://doi.org/10.1111/j.1365-313X.2011.04671.x

Ranf, S., Gisch, N., Schäffer, M., Illig, T., Westphal, L., Knirel, Y.A., Sánchez-Carballo, P.M., Zähringer, U., Hückelhoven, R., Lee, J., Scheel, D., 2015. A lectin S-domain receptor kinase mediates lipopolysaccharide sensing in Arabidopsis thaliana. Nat. Immunol. 16, 426–433. https://doi.org/10.1038/ni.3124

Renelli, M., Matias, V., Lo, R.Y., Beveridge, T.J., 2004. DNA-containing membrane vesicles of Pseudomonas aeruginosa PAO1 and their genetic transformation potential. Microbiology 150, 2161–2169. https://doi.org/10.1099/mic.0.26841-0

Ritbamrung, O., Inthima, P., Ratanasut, K., Sujipuli, K., Rungrat, T., Buddhachat, K., 2025. Evaluating Xanthomonas oryzae pv. oryzae (*Xoo*) infection dynamics in rice for distribution routes and environmental reservoirs by molecular approaches. Sci. Rep. 15, 1408. https://doi.org/10.1038/s41598-025-85422-3

Sartorio, M.G., Pardue, E.J., Feldman, M.F., Haurat, M.F., 2021. Bacterial Outer Membrane Vesicles: From Discovery to Applications. Annu. Rev. Microbiol. 75, 609–630. https://doi.org/10.1146/annurev-micro-052821-031444

Schaar, V., De Vries, S.P.W., Perez Vidakovics, M.L.A., Bootsma, H.J., Larsson, L., Hermans, P.W.M., Bjartell, A., Mörgelin, M., Riesbeck, K., 2011. Multicomponent Moraxella catarrhalis outer membrane vesicles induce an inflammatory response and are internalized by human epithelial cells: Characterization of M. catarrhalis OMVs. Cell. Microbiol. 13, 432–449. https://doi.org/10.1111/j.1462-5822.2010.01546.x

Schwechheimer, C., Kuehn, M.J., 2015. Outer-membrane vesicles from Gram-negative bacteria: biogenesis and functions. Nat. Rev. Microbiol. 13, 605–619. https://doi.org/10.1038/nrmicro3525

Sidhu, V.K., Vorhölter, F.-J., Niehaus, K., Watt, S.A., 2008. Analysis of outer membrane vesicle associated proteins isolated from the plant pathogenic bacterium Xanthomonas campestris pv. campestris. BMC Microbiol. 8, 87. https://doi.org/10.1186/1471-2180-8-87

Smokvarska, M., Francis, C., Platre, M.P., Fiche, J.-B., Alcon, C., Dumont, X., Nacry, P., Bayle, V., Nollmann, M., Maurel, C., Jaillais, Y., Martiniere, A., 2020. A Plasma Membrane Nanodomain Ensures Signal Specificity during Osmotic Signalling in Plants. Curr. Biol. 30, 4654-4664.e4. https://doi.org/10.1016/j.cub.2020.09.013

Solé, M., Scheibner, F., Hoffmeister, A.-K., Hartmann, N., Hause, G., Rother, A., Jordan, M., Lautier, M., Arlat, M., Büttner, D., 2015. Xanthomonas campestris pv. vesicatoria Secretes Proteases and Xylanases via the Xps Type II Secretion System and Outer Membrane Vesicles. J. Bacteriol. 197, 2879–2893. https://doi.org/10.1128/JB.00322-15

Steinhorst, L., He, G., Moore, L.K., Schültke, S., Schmitz-Thom, I., Cao, Y., Hashimoto, K., Andrés, Z., Piepenburg, K., Ragel, P., Behera, S., Almutairi, B.O., Batistič, O.,

Wyganowski, T., Köster, P., Edel, K.H., Zhang, C., Krebs, M., Jiang, C., Guo, Y., Quintero, F.J., Bock, R., Kudla, J., 2022. A Ca2+-sensor switch for tolerance to elevated salt stress in Arabidopsis. Dev. Cell 57, 2081-2094.e7. https://doi.org/10.1016/j.devcel.2022.08.001

Subramoni, S., Pandey, A., Vishnu Priya, M.R., Patel, H.K., Sonti, R.V., 2012. The ColRS system of *Xanthomonas oryzae* pv. *oryzae* is required for virulence and growth in iron-limiting conditions. Mol. Plant Pathol. 13, 690–703. https://doi.org/10.1111/j.1364-3703.2011.00777.x

Sun, X., Parker, J.E., Yu, G., 2025. Phytobacterial effectors antagonize plant reproduction: new weapons in hand. Trends Plant Sci. S1360138525000354. https://doi.org/10.1016/j.tplants.2025.02.001

Thomas, N.C., Schwessinger, B., Liu, F., Chen, H., Wei, T., Nguyen, Y.P., Shaker, I.W.F., Ronald, P.C., 2016. XA21-specific induction of stress-related genes following *Xanthomonas* infection of detached rice leaves. PeerJ 4, e2446. https://doi.org/10.7717/peerj.2446

Tian, W., Hou, C., Ren, Z., Wang, C., Zhao, F., Dahlbeck, D., Hu, S., Zhang, L., Niu, Q., Li, L., Staskawicz, B.J., Luan, S., 2019. A calmodulin-gated calcium channel links pathogen patterns to plant immunity. Nature 572, 131–135. https://doi.org/10.1038/s41586-019-1413-y

Tran, T.M., Chng, C.-P., Pu, X., Ma, Z., Han, X., Liu, X., Yang, L., Huang, C., Miao, Y., 2022. Potentiation of plant defense by bacterial outer membrane vesicles is mediated by membrane nanodomains. Plant Cell 34, 395–417. https://doi.org/10.1093/plcell/koab276

Vogel, J., 2008. Unique aspects of the grass cell wall. Curr. Opin. Plant Biol. 11, 301–307. https://doi.org/10.1016/j.pbi.2008.03.002

Yang, J.-T., Tan, Z.-M., Jiang, Y.-T., Bai, Y.-X., Zhang, Y.-J., Xue, H.-W., Xu, T.-D., Dong, T., Lin, W.-H., 2025. Non-adapted bacterial infection suppresses plant reproduction. Sci. Adv. 11, eads7738. https://doi.org/10.1126/sciadv.ads7738

Zhao, Y., Araki, S., Wu, J., Teramoto, T., Chang, Y.-F., Nakano, M., Abdelfattah, A.S., Fujiwara, M., Ishihara, T., Nagai, T., Campbell, R.E., 2011. An Expanded Palette of Genetically Encoded Ca^{2+} Indicators. Science 333, 1888–1891. https://doi.org/10.1126/science.1208592

Table1: Notable proteins found in purified *Xoo*-OMVs have been presented as a table below:

Table 1: Important proteins identified in Xoo-OMVs

Accession no.	Description	Gene name	Subcellular localization	Unique peptides
Pathogen/microbe-associated molecular patterns				
Q5GZN6	Flagellin	*fliC*	Extracellular	4
Q5GZN5	Flagellar hook-associated protein 2	*fliD*	Extracellular	4
Q5GZP2	Flagellar basal-body rod protein FlgG	*flgG*	Extracellular	4
Q5GZP5	Flagellar hook protein FlgE	*flgE*	Extracellular	4
Q5GZN8	Flagellar hook-associated protein 1	*flgK*	Extracellular	4
Q5GZN7	Flagellar protein	*flgL*	Extracellular	4
Q5GWR8	Elongation factor Tu	*tuf1*	Cytoplasmic	33
Q5GWS9	Elongation factor G	*fusA*	Cytoplasmic	40
Q5H1E1	Elongation factor Ts	*tsf*	Cytoplasmic	22
Cell wall-degrading enzymes				
Q5GVK0	Endoglucanase	*engXCA*	Unknown	2
Q5GU51	Predicted esterase of the alpha-beta hydrolase superfamily	*rssA*	Unknown	2
Q5H683	Cellulase	*egl*	Cytoplasmic Membrane	6
Q5GVI3	cellulase	*XOO4036*	Unknown	4
Q5H3Z0	Cellulase S	XOO1077	Extracellular	4
Q5GZB8	Polygalacturonase	pglA	Extracellular	4
Q5GXE7	Lipase esterase	*estA*	Unknown	2
Q5GVI4	Glucanase	*celA*	Extracellular	4
Other virulence-associated proteins				
Q5H6N5	VirK protein	virK	Unknown	2
Q5GWI2	3-phytase	*phy*	Unknown	2
Q5H4M4	Adhesin	*xadA*	Outer Membrane	4
Q5GZ04	Regulator of pathogenicity factors	*rpfN*	Outer Membrane	4
Q5GYV5	Aconitate hydratase B	*acnB*	Cytoplasmic	24
Q5H0Q6	Phosphoenolpyruvate synthase	*ppsA*	Cytoplasmic	18
Q5GVR9	Tail-specific protease	*prc*	Cytoplasmic Membrane	6
Q5GXA2	Phosphoglycerate kinase	*pgk*	Cytoplasmic	6
Q5GVY3	Thiol:disulfide interchange protein	*dsbA*	Periplasmic	2
Q5GV20	Outer membrane protein beta-barrel domain-containing protein	*ax21*	Outer Membrane	3
Q5H4L8	Type II secretion system core protein G	xpsG	Cytoplasmic Membrane	4
ROS protection				
Q5H243	DNA-binding ferritin-like protein (Oxidative damage protectant)	dps	Cytoplasmic	7
Q5GWL8	Transaldolase	tal	Cytoplasmic	14
Q5GU87	Superoxide dismutase [Cu-Zn]	yojM	Periplasmic	4
I1SB40	Succinate dehydrogenase flavoprotein subunit	sdhA	Cytoplasmic Membrane	6
Q5GXT8	NADH-quinone oxidoreductase	nuoG	Cytoplasmic	13
Q5GWM2	Alkyl hydroperoxide reductase C	ahpC	Cytoplasmic	18
Q5H6Y9	Enoyl-[acyl-carrier-protein] reductase [NADH]	fabV	Cytoplasmic	6
Q5GXU3	NADH-ubiquinone oxidoreductase NQO12 subunit	nuoL	Cytoplasmic Membrane	5
Q5GXT7	NADH-quinone oxidoreductase subunit F	nuoF	Cytoplasmic	8
Q5GUB3	Organic hydroperoxide resistance protein	ohr	Cytoplasmic	9
Q5H1C6	Nitrous oxidase accessory protein	NosD	Unknown	

Phosphate acquisition

Q5H5U3	Two-component system regulatory protein	*phoP*	Cytoplasmic	6
Q5H005	Phosphate-binding protein	*pstS*	Periplasmic	2
Q5H3V1	Polyphosphate-selective porin O	*oprO*	Outer Membrane	2
Q5H4B5	Inorganic pyrophosphatase	ppa	Cytoplasmic	6
Q5GZ07	Multiphosphoryl transfer protein	fruB	Cytoplasmic	11

Iron acquisition

Q5H358	Citrate-dependent iron transporter	*fecA*	Outer Membrane	3
Q5H353	Ferric enterobactin receptor	*bfeA*	Outer Membrane	3
Q5H6Z9	Iron transporter	*yncD*	Outer Membrane	3
Q5H6B6	Outer membrane receptor proteins, mostly Fe transport	*cirA*	Outer Membrane	4
Q5GUH3	Outer membrane receptor for ferrienterochelin and colicins	*fepA*	Outer Membrane	4
Q5H1Y3	TonB-dependent receptor	*iroN*	Outer Membrane	4
Q5H3W8	TonB-dependent receptor	*fyuA*	Outer Membrane	4
Q5H4B7	TonB-dependent receptor	*btuB*	Outer Membrane	4
Q5H4K6	Iron receptor	bfrC	Outer Membrane	3
Q5GV70	Bacterioferritin	*bfr*	Cytoplasmic	14

Type IV secretion system

Q5H1R3	Tfp pilus assembly protein	pilE	Unknown	2
Q5H3Q6	Fimbrial assembly protein	pilQ	Outer Membrane	2
Q5GZT4	Fimbrial biogenesis protein	pilF	Outer Membrane	3
Q5H218	Pilus biogenesis protein	pilJ	Cytoplasmic Membrane	6
Q5H3Q7	Fimbrial assembly protein	pilP	Cytoplasmic Membrane	4
Q5H2I1	Pilin	pilE	Extracellular	4

Type VI secretion system

Q5GX37	Type VI secretion system contractile sheath large subunit	XOO3480	Cytoplasmic	13
Q5GX31	Type VI secretion system tip protein	vgrG	Unknown	2
Q5GX38	Type VI secretion system tube protein	hcp	Extracellular	4
Q5GX43	Gp5/Type VI secretion system Vgr protein OB-fold domain-containing protein	VgrG	Cytoplasmic	8

Tol-Pal proteins

Q5H299	Tol-Pal system protein	tolB	Periplasmic	7
I1SB47	TolC protein	tolC	Outer Membrane	4
Q5H707	Biopolymer transport protein	exbB	Cytoplasmic Membrane	6
Q5H2A2	Tol-Pal system protein TolQ	tolQ	Cytoplasmic Membrane	6

Lipoprotein

Q5H2Q1	Predicted outer membrane lipoprotein	XOO1516	Unknown	2
Q5H2G2	Lipoprotein	XOO1605	Unknown	2
Q5H2Q6	Peptidoglycan-associated outer membrane lipoprotein	pcp	Unknown	2
Q5H3Z9	Outer membrane protein Slp	slp	Outer Membrane	4
Q5GYL4	Lipoprotein	nlpD	Outer Membrane	3
Q5GW29	Lipoprotein	LppC	Outer Membrane	3
Q5H298	Peptidoglycan-associated lipoprotein	ompP6	Outer Membrane	3
Q5H661	Lipoprotein	vacJ	Outer Membrane	3
Q5GVT2	Predicted periplasmic or secreted lipoprotein	OsmY	Periplasmic	2
Q5H2Y8	Predicted outer membrane lipoprotein	XOO1429	Unknown	2
Q5GYP5	Lipoprotein	NlpB	Unknown	2
Q5GVS8	Predicted outer membrane lipoprotein	XOO3941	Unknown	2
Q5GXI9	LPS-assembly lipoprotein LptE	rlpB	Unknown	2
Q5H5W6	Lipoprotein	XOO0400	Unknown	2
Q5H1N7	Lipoprotein	XOO1880	Unknown	2
Q5H263	Lipoprotein	XOO1704	Unknown	2

DSF processing proteins

Q5H4I4	3-oxoacyl-[acyl-carrier-protein] synthase 2	fabF	Cytoplasmic Membrane	6
Q5GXJ7	Oar protein	oar	Outer Membrane	4
Q5H4C1	Ketol-acid reductoisomerase (NADP(+))	ilvC	Cytoplasmic	16

Outer membrane proteins

Q5H1E9	Outer membrane protein assembly factor BamA	oma	Outer Membrane	4
Q5GTY7	Outer membrane protein	ompP1	Outer Membrane	4
Q5H4U1	Outer membrane protein	uptE	Outer Membrane	4
Q5GZT7	Outer membrane protein assembly factor BamB	bamB	Outer Membrane	4
Q5H4Z2	Outer membrane protein W	OmpW	Outer Membrane	3
Q5GVL3	Salt-induced outer membrane protein	XOO4006	Outer Membrane	3
Q5H3Z9	Outer membrane protein Slp	slp	Outer Membrane	3
Q5H2H1	Outer membrane protein assembly factor BamD	comL	Outer Membrane	3
Q5H4L0	General secretion pathway protein D	xpsD	Outer Membrane	3
Q5GWC2	LPS-assembly protein LptD	lptD	Outer Membrane	3
Q5H191	Outer membrane protein assembly factor BamE	smpA	Outer Membrane	3
Q5GVV7	HmsH protein	hmsH	Outer Membrane	3

Figure legends:

Figure 1. Characterization of *Xoo*-OMVs and identification of their protein content. a, AFM images showing the release of BXO43 OMVs into their surroundings by blebbing. b, AFM image of spherical *Xoo*-OMVs. c, the hydrodynamic size range of the *Xoo*-OMVs (125.8 +/- 1.6 nm) exhibited by NTA. d, Transmission electron microscopy image of *Xoo*-OMVs, including smaller vesicles (10-60nm), indicated by the yellow arrow, and bigger vesicles (100-150nm), indicated by the white arrow. e, Subcellular localization of 423 proteins identified from *Xoo*-OMVs proteomic analysis of the Xoo-OMVs (n=4). The localizations were designated using PSortB software. f and g, predicted biological and molecular functions of the proteins identified through proteomic analysis (n=4), appointed using ShinyGo software, are represented in bar charts.

Figure 2. *Xoo*-OMVs induce cellular Ca^{2+} elevation in rice roots. a and b, 7-day-old Khitish and CR 800 roots, respectively, stained with Calcium Green-1, AM, showing an increase in cellular Ca^{2+} when treated with *Xoo*-OMVs. No Ca^{2+} elevation was observed with solvent treatment, scale bar = 125 μm. c and d, the relative fluorescence of the Khitish and CR 800 roots after treatment with *Xoo*-OMVs and solvent control was plotted as a histogram at intervals of 5 minutes using GraphPad Prism software. Student's t-test was done to deduce the statistical difference between the fluorescence of control and *Xoo*-OMV-treated roots at each time point, n= 6 independent replicates. e, the relative expression of the *PR10b* gene after incubation in *Xoo*-OMVs for 1 hour (in the presence and absence of Ca^{2+} chelator) in CR 800 and Khitish roots, (n= 3 independent replicates). The statistical differences have been calculated through one-way ANOVA using GraphPad Prism software (ns, not significant, *P ≤ 0.05; **P ≤ 0.01, ***P ≤ 0.001, ****P ≤ 0.0001).

Figure 3 Ca^{2+} and sterol-dependent lipid order increase in rice plasma membrane after incubation in *Xoo*-OMVs. a, 7-day-old Khitish and CR 800 seedlings incubated with *Xoo*-OMVs for 30 min and stained with Di-4-ANEPPDHQ showing an increase in the lipid order of rice plasma membrane (n ≥ 6 seedlings). Pre-treatment with BAPTA-AM (25 μM) and EGTA (2 mM), respectively, inhibits lipid order increase. b, GP values (-1 to +1) have been calculated using ImageJ software and plotted in a Box-plot using GraphPad Prism software, the corresponding statistical significance have been calculated through one-way ANOVA, (p ≤0.05), c, leaf protoplasts isolated from Khitish and CR 800 showing lipid order rise after incubation with *Xoo*-OMVs. BAPTA-AM (25 μM) and MβCD (2 mM) pre-treated protoplasts not showing significant rise in lipid order even after *Xoo*-OMV exposure. d, GP values of the protoplast membrane of Khitish and CR 800, represented in a box plot. The statistical significance has been calculated by one-way ANOVA using GraphPad Prism software (ns, not significant, *P ≤ 0.05; **P ≤ 0.01, ***P ≤ 0.001, ****P ≤ 0.0001).

Figure 4. *Xoo*-OMVs get inserted into the plasma membrane of rice. a, 7-day-old Khitish and CR 800 roots showing a significant decrease in *Xoo*-OMV insertion on Ca^{2+}-chelation and sterol-depletion with BAPTA-AM (25 μM) and MβCD (2 mM), respectively (n ≥ 7 seedlings), scale bar= 20 μm. b, histogram showing the statistical difference between the relative fluorescence units of each sample, calculated using one-way ANOVA by GraphPad Prism. c, FM4-64 stained *Xoo*-OMVs inserted into the plasma membrane of leaf protoplasts with and without pre-treatment with BAPTA-AM (25 μM). d, GraphPad Prism was used to create the histograms and analyze the statistical difference between the protoplast samples through one-

way ANOVA, (ns, not significant, *P ≤ 0.05; **P ≤ 0.01, ***P ≤ 0.001, ****P ≤ 0.0001). e, the relative fluorescence units of Khitish and CR 800 after *Xoo*-OMV insertion have been compared in a histogram.

Figure 5: *Xoo*-OMVs are perceived through a Ca^{2+}-dependent nandomain-mediated signalling in rice.

Figures:

Figure 1.

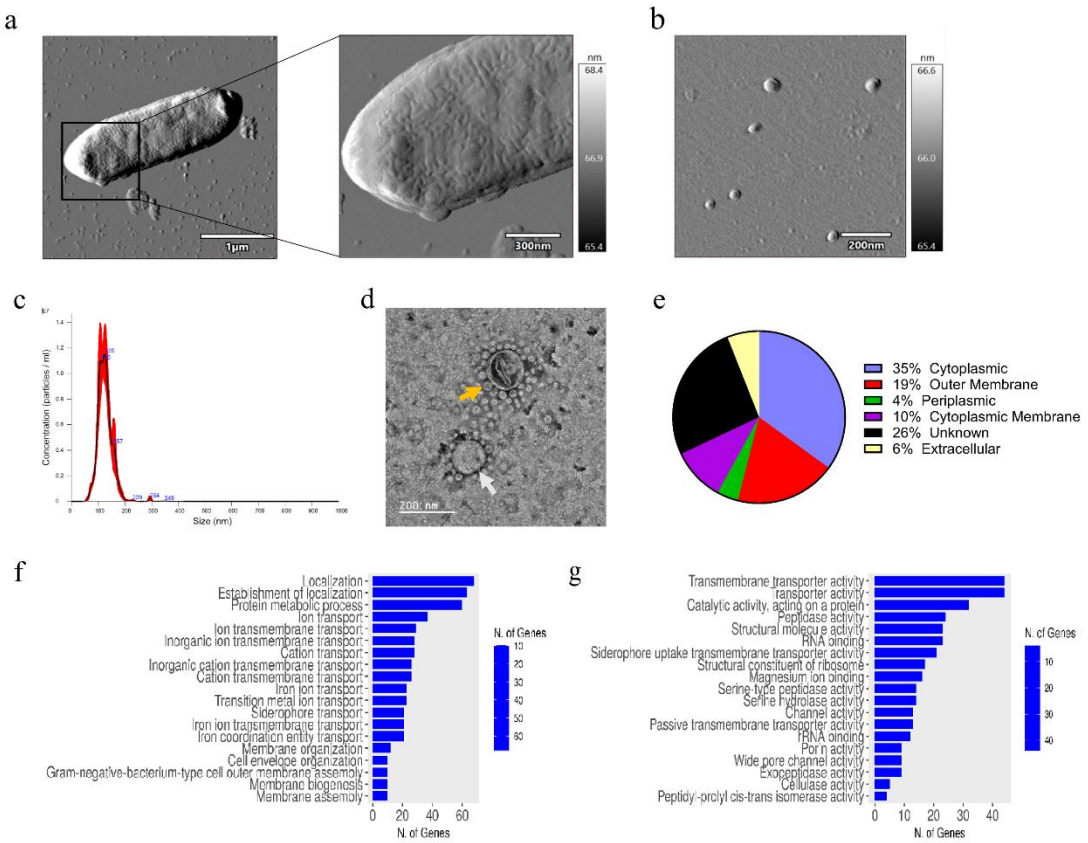

Figure 2.

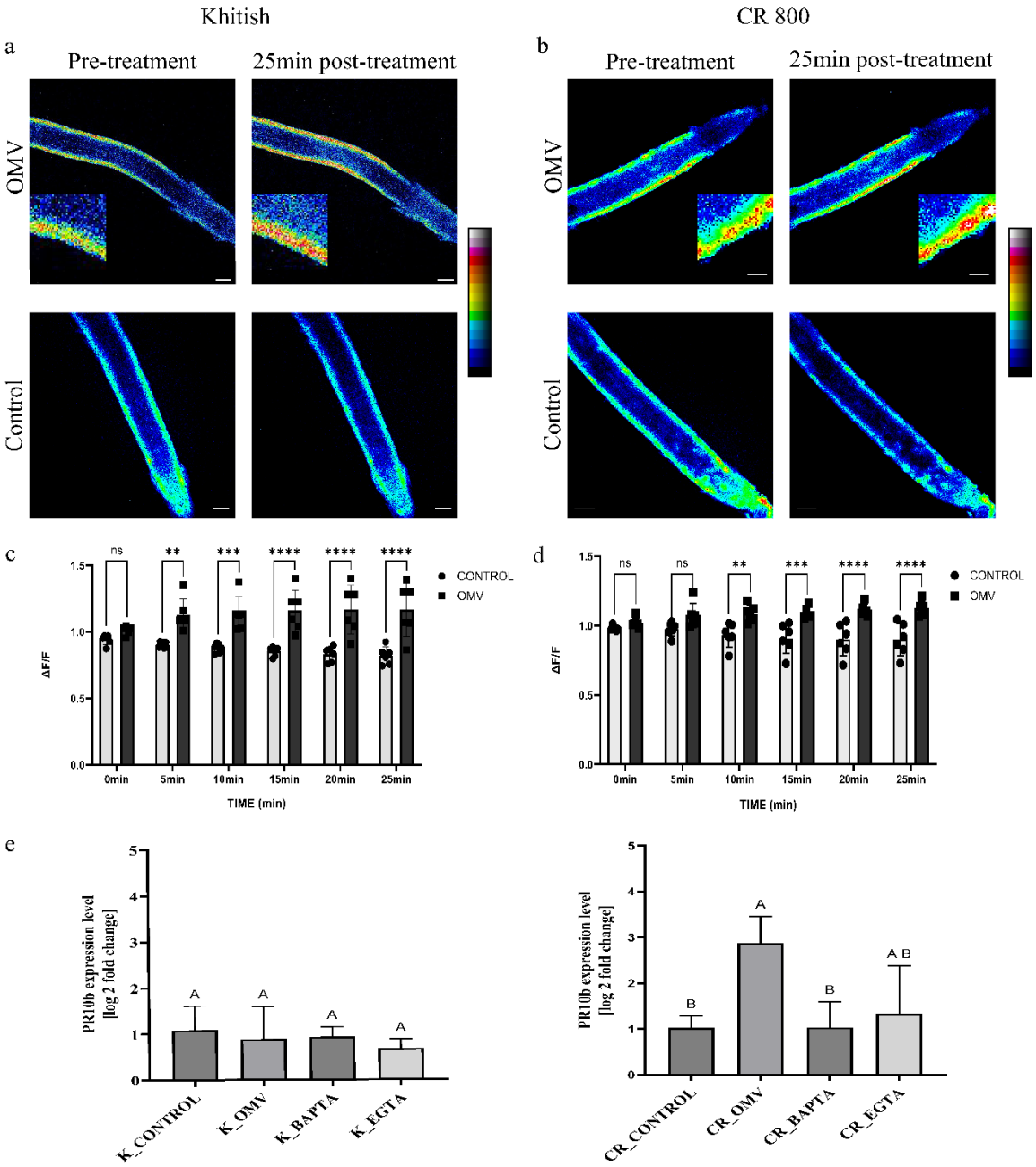
Khitish
CR 800
a
b
Pre-treatment
25min post-treatment
OMV
Control
c
d
ΔF/F
TIME (min)
0min
5min
10min
15min
20min
25min
CONTROL
OMV
ns
**
***
****
e
PR10b expression level
[log 2 fold change]
K_CONTROL
K_OMV
K_BAPTA
K_EGTA
CR_CONTROL
CR_OMV
CR_BAPTA
CR_EGTA

Figure 3.

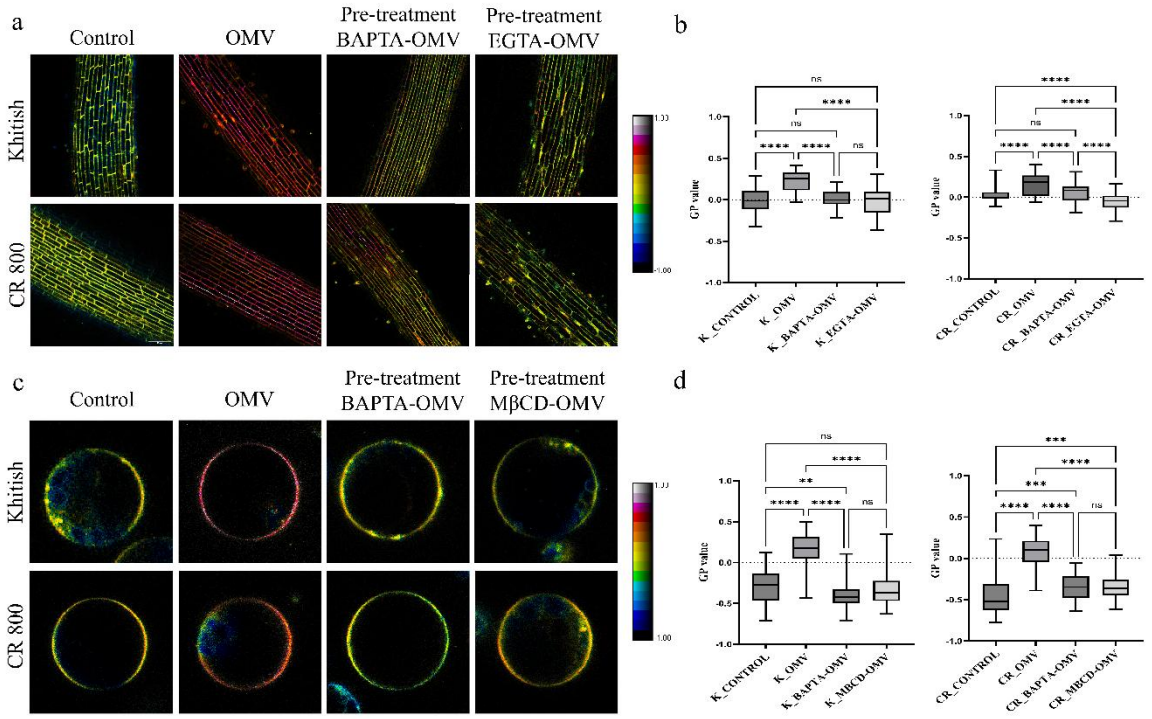

Figure 4.

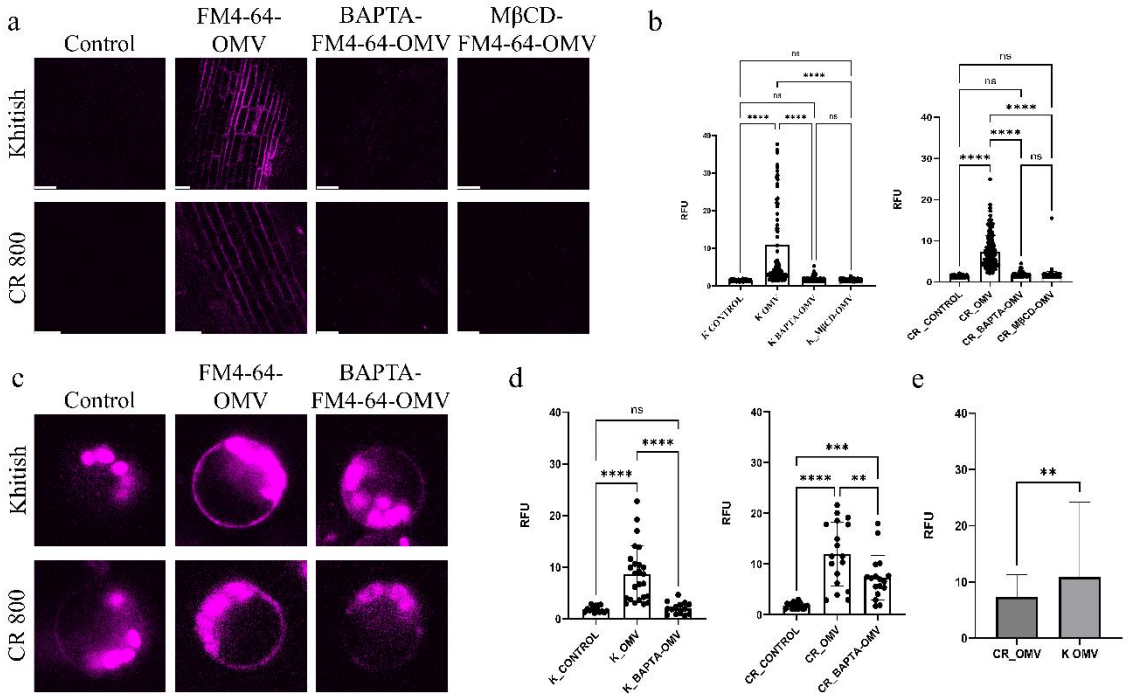

Figure 5.

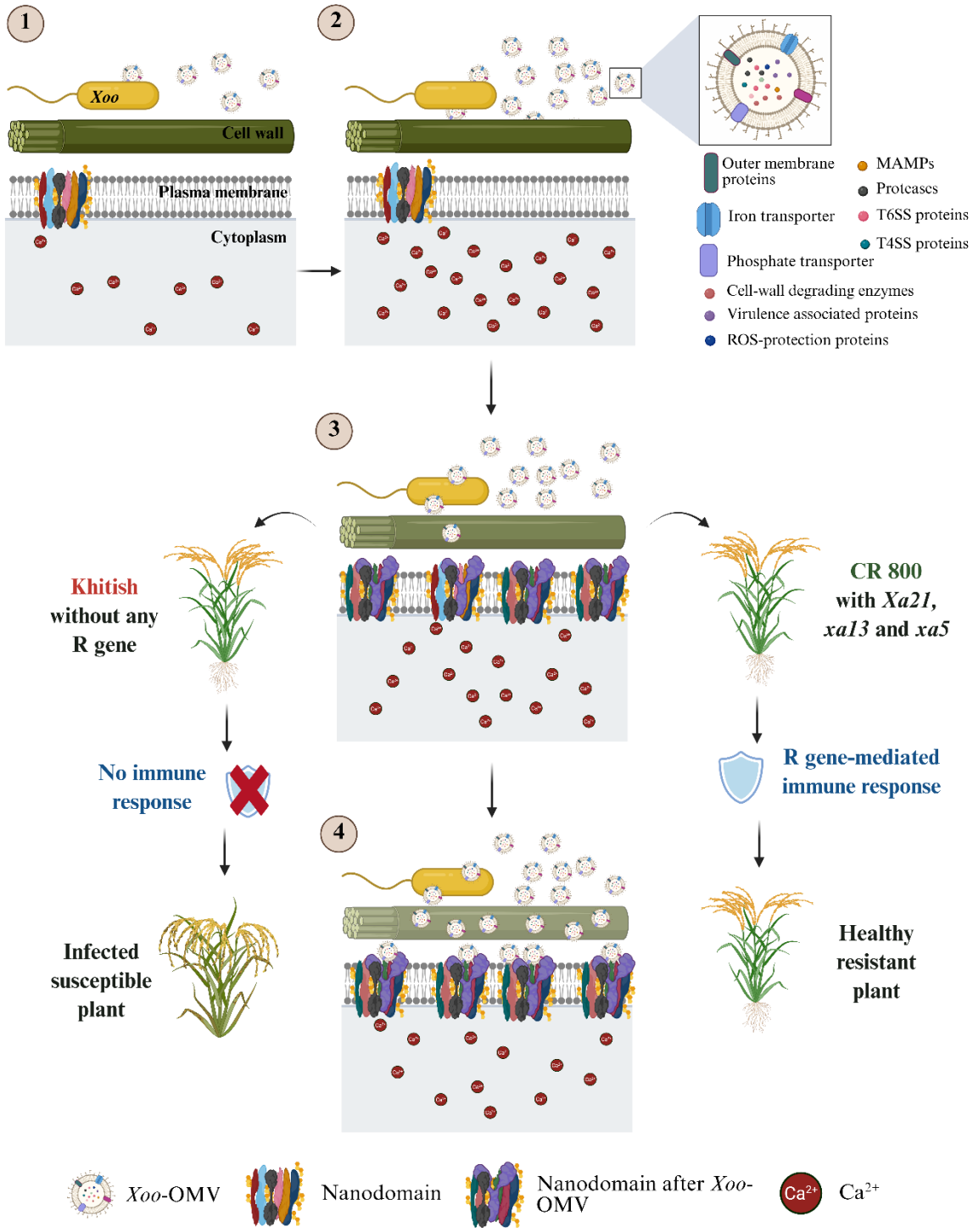
1
2
3
4
Xoo
Cell wall
Plasma membrane
Cytoplasm
Outer membrane proteins
Iron transporter
Phosphate transporter
Cell-wall degrading enzymes
Virulence associated proteins
ROS-protection proteins
MAMPs
Protcases
T6SS proteins
T4SS proteins
Khitish without any R gene
No immune response
Infected susceptible plant
CR 800 with Xa21, xa13 and xa5
R gene-mediated immune response
Healthy resistant plant
Xoo-OMV
Nanodomain
Nanodomain after Xoo-OMV
Ca2+
Ca2+